ISSN: 2476-6909; Modares. Mech. Eng. *2026;26(09):733-742.*

Modares Mechanical Engineering

DOI: 10.48311/mme.2026.118877.82954
journal homepage: mme.modares.ac.ir

Application of multi-scale methods for Lamb wave propagation analysis in a steel beam

Fateme Imani [1,2] , Mahnaz Shamshirsaz[1*] , Mohammad Mohammadi Aghdam [2]

[1] New Technologies Research Center, Amirkabir University of Technology, Tehran, Iran
[2]Department of Mechanical Engineering, Amirkabir University of Technology, Tehran

ARTICLE INFO

Article Type
Original Research

Article History
Received: February 24, 2026
Revised: April 14, 2026
Accepted: May 08, 2026
ePublished: June 20, 2026

ABSTRACT

This study investigates the propagation behavior of Lamb waves in a steel beam at varying inter-sensor distances, employing CWT, FFT, and STFT to evaluate their effectiveness for time–frequency and energy-based signal characterization. Results show that the Lamb-wave time-of-flight exhibits minimal variation despite changes in sensor spacing, yielding a nearly constant group velocity of approximately 4540 m/s, which confirms the stable propagation of the S_0 mode. Multiscale wavelet analysis reveals that nearly 90% of the total energy is concentrated in Scale-1, while the combined contribution of Scales 2–5 remains below 10%, indicating a dominant, low-dispersion single-mode response.Quantitative CWT-based indicators also show consistent trends with increasing distance. Wavelet energy increases by about 20%, whereas entropy decreases from 0.4908 to 0.4651, reflecting stronger energy localization in Scale-1 and improved separation of the S_0 mode from background noise and secondary modes. The RMS value increases from 0.2199 to 0.239, suggesting reduced attenuation and lower dispersion along the propagation path. The reduction in kurtosis further indicates diminished impulsive peaks, increased waveform smoothness, and an enhanced signal-to-noise ratio. Overall, the findings demonstrate that CWT provides superior capability over FFT and STFT in analyzing energy evolution, attenuation characteristics, and time–frequency dynamics of guided waves. These advantages establish CWT as a robust quantitative tool for structural health monitoring and guided-wave analysis.

Keywords: Method of multi-scale, Lamb wave, Time-frequency analysis, Continuous wavelet Transform.

How to cite this article
Imani F, Shamshirsaz M, Mohammadi Aghdam.M, Application of multi-scale methods for Lamb wave propagation analysis in a steel beam. Modares Mechanical Engineering; *2026;26(09):733-742.*

*Corresponding author's email: shamshir@aut.ac.ir
*Corresponding ORCID ID: 0000-0002-4400-4930

شاپا: ۷۹۰۹-۲۴۷۶؛ مهندسی مکانیک مدرس. ۷۴۲-۷۳۳:(۰۹)۲۶;۱۴۰۵

مهندسی مکانیک مدرس

DOI: 10.48311/mme.2026.118877.82954

صفحه اصلی مجله: mme.modares.ac.ir

کاربرد روش حل چندمقیاسی جهت تحلیل انتشار امواج لمب در تیر فولادی

فاطمه ایمانی [۱و۲]، مهناز عبدا... شمشیرساز [۱*]، محمد محمدی اقدم [۲]

[۱] پژوهشکده فناوری نو، دانشگاه صنعتی امیرکبیر، تهران، ایران

[۲] دانشکده مهندسی مکانیک، دانشگاه صنعتی امیرکبیر، تهران، ایران

اطلاعات مقاله

نوع مقاله

مقاله پژوهشی

تاریخچه مقاله

دریافت: ۱۴۰۴/۱۲/۰۵

بازنگری: ۱۴۰۵/۰۱/۲۵

پذیرش: ۱۴۰۵/۰۲/۱۸

ارائه آنلاین: ۱۴۰۵/۰۳/۳۰

چکیده

این پژوهش به بررسی رفتار انتشار امواج لمب در یک تیر فولادی تحت تغییر فاصله حسگرهای پیزوالکتریک پرداخته و با استفاده از سه روش CWT، FFT و STFT، کارایی آن‌ها در تحلیل ویژگی‌های زمانی–فرکانسی و انرژی موج بررسی شده است. نتایج نشان می‌دهد که زمان‌پرواز امواج لمب با وجود تغییر فاصله، کمترین نوسان را داشته و سرعت گروهی تقریباً ثابت و برابر با 4540 m/s به‌دست آمد که بیانگر پایداری انتشار مود S_0 است. تحلیل چندمقیاسی سیگنال نشان داد؛ که حدود ۹۰٪ انرژی کل در Scale-1 متمرکز بوده و مجموع انرژی Scale-2 تا Scale-5 کمتر از ۱۰٪ است؛ بنابراین موج غالب دریافت‌شده دارای رفتار تک مودی و کم پراکنش است. شاخص‌های کمی استخراج‌شده از CWT نیز روندهای سازگار با افزایش فاصله را نشان دادند. انرژی موجک با افزایش فاصله حدود ۲۰٪ افزایش یافت، درحالی‌که آنتروپی از ۰/۴۹۰۸ به ۰/۴۶۵۱ کاهش پیدا کرد که نشان‌دهنده تمرکز بیشتر انرژی در Scale-1 و تفکیک مناسب مود S_0 از نویز و مودهای جانبی است. مقدار RMS از ۰/۲۱۹۹ به ۰/۲۳۹ افزایش یافت که حاکی از کاهش اتلاف انرژی و پاشندگی کمتر موج در مسیر انتشار است. همچنین کاهش کورتوزیس بیانگر کاهش پیک‌های ضربه‌ای، افزایش یکنواختی شکل موج و بهبود نسبت سیگنال به نویز است. در مجموع، یافته‌ها نشان می‌دهد که روش CWT نسبت به FFT و STFT توانایی بالاتری در تحلیل انرژی، میرایی و ساختار زمان–فرکانس امواج هدایت‌شده دارد و می‌تواند به‌عنوان یک ابزار کمی و کارآمد در پایش سلامت سازه به‌کار رود.

کلیدواژه‌ها: روش حل چندمقیاسی، امواج لمب، تحلیل زمان- فرکانس، تبدیل موجک پیوسته

نحوه ارجاع به این مقاله

ایمانی فاطمه،عبدا... شمشیرساز مهناز ، محمدی اقدم محمد،کاربرد روش حل چندمقیاسی جهت تحلیل انتشار امواج لمب در تیر فولادی ، مهندسی مکانیک مدرس. ۷۴۲-۷۳۳:(۰۹)۲۶;۱۴۰۵

*پست الکترونیکی نویسنده عهده‌دار مکاتبات: shamshir@aut.ac.ir

*شناسه ارکید نویسنده عهده‌دار مکاتبات: 0000-0002-4400-4930

1- Introduction

Lamb waves are a class of ultrasonic guided waves propagating in plate- and beam-like structures, which are widely employed in nondestructive testing (NDT) and structural health monitoring (SHM) due to their ability to interrogate large areas with relatively low attenuation and high sensitivity to defects. A comprehensive theoretical and practical foundation for Lamb waves and ultrasonic guided waves is provided in the classical monograph by Rose [1], which established the essential roles of dispersion, mode selection, and wave–structure interaction in ultrasonic inspection applications.

Moreover, the level of development for the theory is comparatively high, it is due to some of the most difficult problems regarding signal analyses within the time domain and experiments. The Lamb wave problem ranks amongst the few that are multi-modal. Classical Theory of Lamb waves primarily addresses the development of the Rayleigh-Lamb wave equation. Relations of dispersion, which describe the phase and group velocities of waves, were at first developed by Rayleigh, [2], later corrected by Lamb, [3]. Accordingly, the authors can consider using a different model based on different technique, and other variables, concerning the outcome of the analysis for the lamb wave. However, as emphasized by Viktorov [4] and Lowe [5], dispersion curves alone do not describe how wave amplitudes and envelopes evolve during propagation, particularly for finite-duration excitations .At smaller length scales, accurate theoretical modeling becomes essential to capture size-dependent wave phenomena. Ghodrati et al. presented an analytical study of Lamb wave dispersion in aluminum nitride micro-plates based on the consistent couple stress theory. Their work emphasized the significant role of micro-scale effects in guided wave propagation and offered a robust framework for deriving dispersion curves and identifying intrinsic material length-scale parameters [6].

Alongside conventional wave propagation studies, data-driven techniques have increasingly been incorporated into guided wave–based damage detection frameworks. Ziaiefar et al. introduced a practical ultrasonic guided-wave damage classification method for pipes and plates, integrating wavelet-based feature extraction with a support vector machine (SVM) classifier. Their approach achieved high accuracy in differentiating corrosion-related damage from crack-type defects, demonstrating its strong potential for real-world structural health monitoring applications [7]. Also, within practical experiments conducted for ultrasonic waves and their applications, the role of utilizing the harmonics has been recognized as not affecting lamb waves. Furthermore, band-limited burst waves have been developed within the context of the different multiples of waves that may be distorted. With regards to a relevant example and a corresponding phenomenon of wave propagation and scale, a successful method has been identified as the Method of Multi Scale (MST) [8]. The general theoretical foundations of MTS were established in nonlinear dynamics by Nayfeh [9], Kevorkian and Cole [10], who developed a systematic perturbation framework for eliminating secular terms and deriving uniformly valid amplitude evolution equations. Since then, MTS has been extended to a wide range of weakly nonlinear, damped, and forced systems, demonstrating its robustness for long-distance and long-time wave propagation analysis. Then, the usage of MTS tools is applied in the propagation of Lamb Waves, which fall under Ultrasonic Guided Waves. Kanda and Maruyama [11] employed MTS to analyze finite-bandwidth Lamb-wave packets and demonstrated that higher-order asymptotic solutions can explicitly predict symmetric and antisymmetric envelope distortions as well as peak shifts during propagation. Their results showed that the apparent propagation velocity inferred from time-domain peak tracking can deviate from the classical group velocity and that the distortion strength depends on the selected propagation mode, excitation frequency, and initial packet shape. Aside from all the other dispersion forces previously identified as having a possible effect on the guided wave system, there exists other factors that can affect the actual excitation by pulses and transducers, in theory. Addressing this aspect, Kanda and Maruyama [12] developed an MTS-based formulation for forced Lamb waves and derived a solvability condition that reduces the original second-order elastodynamic boundary-value problem to a first-order amplitude evolution equation. By employing Green's function techniques, they demonstrated that modal amplitudes can be efficiently obtained for arbitrary spatiotemporal forcing distributions and revealed a resonance-like behavior governed by the relationship between excitation timing, spatial forcing location, and the group velocity of the propagation mode.

In immersion testing, Kauffmann, Ploix, and Chaix [13-14] investigated multi-modal leaky Lamb waves in parallel immersed plates through a combination of analytical modeling, finite-element simulations, and experimental measurements. Their study showed that leaky Lamb modes can propagate between plates without mode conversion and that apparent attenuation can be reduced due to continuous energy supply, highlighting the importance of amplitude evolution and energy-transfer mechanisms in realistic inspection scenarios. Despite these advances, a unified analytical description that directly links MTS-based amplitude evolution to experimentally measured time-domain signals obtained from piezoelectric transducer setups remains limited. In the task of monitoring Lamb waves on steel beams using surface bound piezoelectric transducers, voltage is measured by an oscilloscope. These signals inherently reflect dispersion-induced waveform distortion, slow amplitude modulation, and forcing effects phenomena that are naturally captured by MTS but are rarely interpreted within a single analytical-experimental framework. In the present work, building upon the MTS-based dispersion analysis of Kanda [15] and the forced-wave framework, the governing elastodynamic equations are expanded using multiple spatial and temporal scales. Concerning the problem of research, the formula of correspondence reduces to the formula of the evolution of the amplitude with respect to time, to the formula of the first order. The process that corresponds to that formula is the appearance of a pattern in time. Through this integration of rigorous asymptotic analysis and experimentally relevant signal interpretation, the method of multi-scale is advanced from a predominantly theoretical tool to a practical and physical tool for ultrasonic Lamb-wave analysis in NDT and SHM applications.

2- Theoretical Formulation

2 -1 Governing equations

The general equations of motion for the case in which lamb waves propagate in an isotropic elastic plate can be obtained from the two-dimensional equation of elastodynamics .

The equations of motion for lamb waves which include the displacement components, are solved. These equations consider the components of longitudinal displacement and the components of transverse displacement. This includes the equation with components of the in-plane displacements u(x, z, t) and the equation with components of the out-of-plane displacements w(x, z,t) [1]. From the partial differential equations mentioned above, the following formulae (1) and (2) can be derived:

$$-\rho\frac{\partial^2}{\partial t^2}u+(\lambda+\mu)\left(\frac{\partial^2}{\partial x^2}u+\frac{\partial^2}{\partial x\partial z}w\right)+\mu\left(\frac{\partial^2}{\partial x^2}u+\frac{\partial^2}{\partial z^2}u\right)=0 \qquad (1)$$

$$-\rho\frac{\partial^2}{\partial t^2}u+(\lambda+\mu)\left(\frac{\partial^2}{\partial z^2}w+\frac{\partial^2}{\partial x\partial z}u\right)+\mu\left(\frac{\partial^2}{\partial x^2}w+\frac{\partial^2}{\partial z^2}w\right)=0 \qquad (2)$$

Strain equations of the second-order modification of the strain-displacement equations are proposed to highlight the significance of the nonlinearity of the dynamics of the waves. The explanation of the proposed theory will be valid based on the fact that it is possible to represent the nonlinearity of the strain using parameter ε_{11} from equations of strain (3).

$$\varepsilon_{11}=(u_{1,1}+\frac{1}{2}u_{1,1}^2)=(\frac{\partial u}{\partial x}+\frac{1}{2}(\frac{\partial u}{\partial x})^2) \quad (3)$$

The strain nonlinearities can be expressed through linear and quadratic forms of the displacement gradient, which play a key role in the propagation of finite-amplitude waves, as it inherently contains the displacement gradient of the guided wave. This behavior can be captured by applying an external force F, as shown in equation (4). This formulation simplifies the analysis of excitation effects induced by a piezoelectric component. Within this framework, forced wave propagation can be studied using the same governing equations, in conjunction with solvability conditions, thereby reducing the elastodynamic problem to the form given in equation [1].

$$\rho\frac{\partial^2 u_i}{\partial t^2}-(\lambda+\mu)\left(\frac{\partial^2 u_k}{\partial x_i \partial x_k}\right)-\mu\left(\frac{\partial^2 u_i}{\partial x_k^2}\right)=F_i \quad (4)$$

All the equations of motion of the wave for the Lamb wave propagating in the elastic plate can be expressed with the two-dimensional equation of elastodynamics, with u and w, as the in-plane displacement and the out-of-plane displacement, respectively in the above equation. The other values of the Lamé parameters can then be calculated based on λ, μ, and ρ, the density. The above equation accounts for non-linear strains as well .

In that case, to facilitate this discourse on the finite amplitude of the lamb waves' effects, it is necessary to refer to the linear and quadratic strains expressed in matrix form. The matrix formula expressing the linear and quadratic gradient of displacement as a function of the given value of the stress component σ_{11}, with constants λ and μ defined as the constants of Lamé, and constants A, B, and C defined as the constants of third-order elasticity or Murnaghan, is given in equation (5).

$$\begin{aligned}\sigma_{11}&=(\lambda+2\mu)\varepsilon_{11}+[(\lambda+2\mu)+(A+3B+C_1)\,\varepsilon_{11}^2\\&=(\lambda+2\mu)(\frac{\partial u}{\partial x}+\frac{1}{2}(\frac{\partial u}{\partial x})^2)+\\&[(\lambda+2\mu)+(A+3B+C)](\frac{\partial u}{\partial x}+2\frac{1}{2}(\frac{\partial u}{\partial x})^2)^2\end{aligned} \quad (5)$$

To substitute the nonlinear equations for the stress components, the equation that defines the motion, taking into account the longitudinal component, will have the following form (6):

$$\begin{aligned}\sigma_{11,1}&=(\lambda+2\mu)(\frac{\partial^2 u(x.t)}{\partial x^2}+\frac{\partial u(x.t)}{\partial x}\frac{\partial^2 u(x.t)}{\partial x^2})\\&+[(\lambda+2\mu)+(A+3B+C)(2\frac{\partial u(x.t)}{\partial x}\frac{\partial^2 u(x.t)}{\partial x^2}+\frac{\partial^2 u(x.t)}{\partial x^2}(\frac{\partial u(x.t)}{\partial x})^3+\\&3\frac{\partial^2 u(x.t)}{\partial x^2}(\frac{\partial u(x.t)}{\partial x})^2)^2\end{aligned} \quad (6)$$

Equation (6) is the reduced form of the motion equation for the one-dimensional case. In this equation, the so-called in-plane displacement approach is adopted. There is the mass-associated part $\rho\frac{\partial^2 u_1}{\partial t^2}$ with the countering effect of the stress gradient force. This is due to the linear elasticity part and the correction part of the formula. In fact, what takes place within the description in the formula is as follows:

$$\rho u_{1,tt}=\rho\frac{\partial^2 u_1(x.t)}{\partial x^2} \quad (7)$$

Finally, there is also another form of solution for the wave field given through an equation. The given equation can be utilized in the multi-scale method, with the provision that the solution to equation (6) in terms of displacement must modulate within a wave packet. The solution to this equation helps considerably in finding the fastest variation solution to the wave field.

The state equations can also be in a generalized form, considering the terms of higher order of the components in the strain, based on the stresses expressed in the relationship [4]. From the above equations, equation (8) will be derived for the wave motion equation:

$$u(x,t)=u(x)\eta(t) \quad (8)$$

However, since the form of the solution to the modulated wave packet is not known, the solution to the multi-scale method is assumed to be in the following form: using the nonlinear equations (6) in the basic equations of elastodynamics, the nonlinear wave equation is derived. The nonlinear wave equation is as follows:

$$\begin{aligned}\sigma_{11,1}&=(\lambda+2\mu)(\frac{\partial^2 u(x)\eta(t)}{\partial x^2}+\frac{\partial u(x)\eta(t)}{\partial x}\frac{\partial^2 u(x)\eta(t)}{\partial x^2})\\&+[(\lambda+2\mu)+(A+3B+C)(2\frac{\partial u(x)\eta(t)}{\partial x}\frac{\partial^2 u(x)\eta(t)}{\partial x^2}+\frac{\partial^2 u(x)\eta(t)}{\partial x^2}(\frac{\partial u(x)\eta(t)}{\partial x})^3+3\frac{\partial^2 u(x)\eta(t)}{\partial x^2}(\frac{\partial u(x)\eta(t)}{\partial x})^2)^2\end{aligned} \quad (9)$$

We are basically dealing here with two forms of linear equations. The manipulation of the following equation of the equation (9) might have resulted in yielding the subsequent equation (10). One important observation in this equation is the explanation of the elastic constant in the form of the equation of motion. The consideration of the linear and nonlinear equations in connection with the equation of motion has its own significance.

$$\begin{aligned}\rho u(x)\frac{\partial^2\eta(t)}{\partial t^2}&=(\lambda+2\mu)\,\eta(t)\frac{\partial^2 u(x)}{\partial x^2}+([3(\lambda+2\mu)+\\&2(A+3B+C)]\,\eta(t)^2\frac{\partial u(x)}{\partial x}\frac{\partial^2 u(x)}{\partial x^2}\\&+[3(\lambda+2\mu)+2(A+3B+C)]\eta(t)^3\frac{\partial^2 u(x)}{\partial x^2}(\frac{\partial u(x)}{\partial x})^2\\&+[(\lambda+2\mu)+(A+3B+C)]\eta(t)^4\frac{\partial^2 u(x)}{\partial x^2}(\frac{\partial u(x)}{\partial x})^3\end{aligned} \quad (10)$$

2 -2 The multi- scale method

The definition of the operators in relations (12) to (14) provides a compact form of equation (10) to have equation (11). In the mathematical explanation of waves motion, the wave operator has been defined previously as the cause of waves propagation, while the explanation of the perturbation operators mentioned before is the cause of the modulation of waves as well.

$$\frac{\partial^2\eta(t)}{\partial t^2}=\Delta_1\,\eta(t)+\Delta_2\,\eta(t)^2+\Delta_3\,\eta(t)^3+\Delta_4\,\eta(t)^4 \quad (11)$$

$$\Delta_1=\frac{(\lambda+2\mu)\frac{\partial^2 u(x)}{\partial x^2}}{\rho u(x)} \quad (12)$$

$$\Delta_2=\frac{[3(\lambda+2\mu)+2(A+3B+C)]\frac{\partial u(x)\partial^2 u(x)}{\partial x\ \partial x^2}}{\rho u(x)} \quad (13)$$

$$\Delta_3=\frac{3[(\lambda+2\mu)+(A+3B+C)]\,(\frac{\partial u(x)}{\partial x})^2\ \frac{\partial^2 u(x)}{\partial x^2}}{\rho u(x)} \quad (14)$$

The operator definitions will be helpful for the further analysis of the governing equation on various scales; thus, the scaled operators, denoted as Δ_1 to Δ_4 and representing the normalized wave operators of the wave equations, are expressed in a compact mathematical form of Eq. (15):

$$\Delta_4=\frac{[(\lambda+2\mu)+(A+3B+C)]\,(\frac{\partial u(x)}{\partial x})^3\ \frac{\partial^2 u(x)}{\partial x^2}}{\rho u(x)} \quad (15)$$

The equations (9) up to the equations (11), form the basis of the strategy for formulating the progressive step-by-step decomposition of the equations of motion into the linear parts and the nonlinear parts. This strategy focuses its key on using the multi-scale methodical strategy approaches to the solutions.

2-2-1 Leading-order solution

It is essential to prioritize solutions according to their relevance to the primary objective, giving the highest importance to the principal or most probable solution [17]. All other solutions should then be ranked relative to this primary solution.

$$\eta_n(T_0,T_1)=\eta_0(T_0,T_1)+\varepsilon\,\eta_1(T_0,T_1) \quad (16)$$

In this case, the sequence of the wave has been ranked according to its relevance to the problem, its diverse forms in time and space, and its relationship to Eq. (17):

$$\eta_n(t)=\eta_n(T_0(t),T_1(t)) \quad (17)$$

$$\frac{d}{dt}=\frac{\partial}{\partial T_0}+\varepsilon\frac{\partial}{\partial T_1}+\varepsilon^2\frac{\partial}{\partial T_2} \quad (18)$$

Using this method, it should also be possible to derive the extended derivative. This derivation can be developed in relation to the expansion, the general form of the problem, its diverse

representations, the different time scales, the procedural steps, the application of the chain rule, the specific form in question, and the time derivative [12].

The equation in terms of multi-scale function representation in the base equation is given in Eq.(19), an addition of equations involving a common order scale of a small parameter ε, making equations in terms of amplitudes:

$$\frac{\partial^2}{\partial T_0^2}\eta_n(T_0.T_1) + 2\varepsilon\frac{\partial^2}{\partial T_0 \partial T_1}\eta_n(T_0.T_1) + \varepsilon^2\frac{\partial^2}{\partial T_1^2}\eta_n(T_0.T_1) = \Delta_1\eta_n(T_0.T_1) + \Delta_2\eta_n(T_0.T_1)^2 + \Delta_3\eta_n(T_0.T_1)^3 + \Delta_4\eta_n(T_0.T_1)^4 \quad (19)$$

2 -2-2 First-order correction and solvability conditions

In order to apply the proposed method to the problem in this study, the identification method is considered for the specific instance described above. To apply the scales, the specified form is introduced within the chosen combination. The application of this form across diverse scales is then examined in the context of the general problem. Consequently, the corresponding identification is performed on the combination, leading to the application of equation (20):

$$\frac{\partial^2}{\partial T_0^2}(\eta_0(T_0.T_1) + \varepsilon\eta_1(T_0.T_1)) + 2\varepsilon\frac{\partial^2}{\partial T_0 \partial T_1}(\eta_0(T_0.T_1) + \varepsilon\eta_1(T_0.T_1) + \varepsilon^2\frac{\partial^2}{\partial T_1^2}(\eta_0(T_0.T_1) + \varepsilon\eta_1(T_0.T_1)) = \Delta_1(\eta_0(T_0.T_1) + \varepsilon\eta_1(T_0.T_1)) + \Delta_2(\eta_0(T_0.T_1) + \varepsilon\eta_1(T_0.T_1))^2 + \Delta_3(\eta_0(T_0.T_1) + \varepsilon\eta_1(T_0.T_1))^3 + \Delta_4(\eta_0(T_0.T_1) + \varepsilon\eta_1(T_0.T_1))^4 \quad (20)$$

Thus, Equation (20) appears to be structured to decompose the main governing equation. This is achieved through a scaled operator representation of the displacement field, expressed as a multi-scale function across different hierarchical levels. In this hierarchy, the highest scale is at least as significant as the wave equation itself, while the remaining scales hold physical importance for analyzing the equation's solution.

The general form of the problem (specifically its zero-order version) is analogous to the classical Lamb wave problem. This analogy guides the identification procedure, but it is important to note that the original problem formulation did not include the force term.

$$\varepsilon^0: \frac{\partial^2}{\partial T_0^2}\eta_0(T_0.T_1) = \Delta_1\eta_0(T_0.T_1) + \Delta_2\eta_0(T_0.T_1)^2 + \Delta_3\eta_0(T_0.T_1)^3 + \Delta_4\eta_0(T_0.T_1)^4 \quad (21)$$

In this scenario, the problem is analyzed relative to the objective by considering higher-order terms. This analysis follows the identification procedure, which is based on the problem's development, the introduced concepts, the identified force term, the specific case studied, and the use of equation (22):

$$\varepsilon^1: \frac{\partial^2}{\partial T_0^2}\eta_1(T_0,T_1) - \Delta_1\eta_1(T_0,T_1) - 2\Delta_2\eta_0(T_0,T_1)\eta_1(T_0,T_1) - 3\Delta_3\eta_0(T_0,T_1)^2\eta_1(T_0,T_1) - 4\Delta_4\eta_0(T_0,T_1)^3\eta_1(T_0,T_1) = -2\frac{\partial^2}{\partial T_0 \partial T_1}\eta_0(T_0,T_1) \quad (22)$$

Equation (22) describes the basic linear wave equation, which involves the field T_0. It describes a classical Lamb wave. The equation involving formula Eq. (23), describes the involvement of modulating factors because it describes an equation involving the second-order time derivative, scaled as order ε^2.

$$\varepsilon^2: 2\frac{\partial^2}{\partial T_0 \partial T_1}\eta_1(T_0,T_1) - \Delta_2\eta_1(T_0,T_1)^2 - 3\Delta_3\eta_1(T_0,T_1)^2\eta_0(T_0,T_1) - 6\Delta_4\eta_1(T_0,T_1)^2\eta_0(T_0,T_1)^2 = -\frac{\partial^2}{\partial T_1^2}\eta_0(T_0,T_1) \quad (23)$$

This involves deriving an evolution equation. The derivation is formulated using enrichment functions to describe the envelope. These functions characterize the envelope's direction and its modulation of the carrier wave in space.

The transport equation states that the spatial derivative of the wave amplitude relates to its time derivative through the group speed, C_g. This fundamentally describes the transport of the wave energy at the group velocity.

$$\varepsilon^3: \frac{\partial^2}{\partial T_1^2}\eta_1(T_0,T_1) - \Delta_3\eta_1(T_0,T_1)^3 - 4\Delta_4\eta_1(T_0,T_1)^3\eta_0(T_0,T_1) = 0 \quad (24)$$

Thus, this method ensures the mathematical solvability required to determine the amplitude evolution. It thereby enables a smooth transition from theoretical models of weak nonlinearity and dispersion to the experimental modulation of a wave packet.

$$\frac{\partial A}{\partial x_1}\frac{1}{C_g}\frac{\partial A}{\partial t_1}\alpha A = 0 \quad (25)$$

To ensure a physically valid solution, the derivation must follow a specific format. This involves using enrichment functions to describe the wave envelope, as outlined in Eq. (26).

$$A(x_1,t_1)A_0\exp(-\alpha x_1)f(t_1-\frac{x_1}{C_g}) \quad (26)$$

In this case, a clear separation must be established to distinguish the admissible wave solution from the physical problem. This boundary distinguishes the amplitude and the carrier frequency modulation of the wave from that in the physical problem's phase-modulated solution [20]. Furthermore, the operation must reconstruct the admissible solution within the spatial region where the measurable displacement is defined:

$$U(x,z,t)\mathrm{R}\{A(x_1,t_1)\phi(z)e^{i(kx-\omega t)}\} \quad (27)$$

Based on Eq. (27), the derivation must produce a formula relating the normalized units of wave attenuation via a logarithmic function. This derivation must also introduce a supplementary parameter to describe the wave packet distortion. The derivation must account for the oscillation phenomena and the development of wave envelopes by adding higher-order perturbation terms, specifically, powers of ε to the admissible solution.

Finally, based on Eq. (27), the derivation must establish a formula that relates the normalized attenuation units through a logarithmic function. It must also introduce a supplementary parameter to model the wave packet's distortion process. Lastly, by adding higher-order perturbation terms (specifically, powers of ε) to the admissible solution, the derivation must account for the oscillation phenomena and the development of wave envelopes.

The final derivation, based on the mathematical form of the admissible solution for the specific equation (requiring terms of order ε^3), must produce a supplementary formula describing the wave packet's motion in terms of group velocity.

2 -3 Short-Time Fourier Transform

The application of the Fast Fourier Transform (FFT) technique is essential for obtaining the time-frequency representation needed to analyze the measurable spectral characteristics of the signal. The primary advantage of applying the FFT technique in this work is its ability to provide a global time-frequency representation of the signal, clearly describing both its temporal form and spectral frequency content. Despite its benefits, the most significant limitation of the FFT technique used in this study is its inability to provide information about the exact frequency values of the signal at specific times. This is demonstrated in the time-domain representation above [1].

Moreover, this technique also cannot provide information about the signal's phase description, as shown in the specific representation above. Fast Fourier Transform (FFT): The FFT method used in this study can calculate this spectral perspective. For this purpose, the discrete Fourier transform of the voltage time function v(t) is given by the following formula:

$$V(t)\alpha A(x_s,t)\cos(\omega t - kx_s),\quad \alpha_{eff}\frac{1}{x}\mathrm{In}(\frac{A(x)}{A(0)}) \quad (28)$$

Conversely, the corresponding time-domain perspective or form of the information is not provided.

The Discrete Fourier Transform (DFT) used in this study provides the spectral representation of the signal. Specifically, the DFT of the voltage time function $v(t)$ is given by the following formula:

$$V(f)=\int_{-\infty}^{\infty} v(t)e\text{-}i2\pi ft \quad dt \tag{29}$$

In this representation, $V(f)$ displays the signal's spectrum, thereby supplying the required frequency-domain information. As the corresponding time-domain representation is not provided, Short-Time Fourier Transform (STFT) can be applied to provide the information about the signal's time-domain. By this technique, the signal is studied in a two-dimensional time-frequency space [1]. The discrete STFT is described by Equation (30):

$$STFT(t,f)=\int_{-\infty}^{\infty} v(\tau)\,\omega(\tau\text{-}t)\,e^{-i2\pi ft}\,d\tau \tag{30}$$

This demonstrates that the specific form effectively depicts the intended signal representation. In this case, the chosen form accurately represents the signal's perspective. Consequently, through this process, the frequency information is developed and localized in time. Concerning Time-Frequency resolution, the trade-off in this method is that the finite window function w(t) governs the time-frequency resolution. A shorter window provides higher time resolution but lower frequency resolution, while a longer window yields higher frequency resolution at the expense of temporal precision. The STFT magnitude, |STFT(t,f)|, makes this a highly effective technique for analyzing non-stationary signals, such as the received ultrasonic Lamb wave packets in this study [1]. Due to dispersion, the frequency content of these wave packets changes slowly over time. In guided wave propagation, dispersive Lamb waves exhibit disturbances, variations in spreading, and amplitude modulations within the wave packets.

The STFT analyzes the dispersion-related variations and patterns in the signal's energy distribution over time. It has proven highly effective in obtaining a clear time-frequency representation of the signal. Furthermore, extracting a large number of parameters from both the time and frequency domains helps determine the relationships between actuators, sensors, and Lamb waves. This approach also enables an objective comparison of wave arrival characteristics, amplitude decay, and energy redistribution processes, while providing a means to validate directly the analytically derived multi-scale formulations. The amplitude evolution formula describes the envelope evolution of the Lamb wave and corresponds to the leading-order solution of the carrier wave equation. A clear representation of each scale facilitates the analysis of experimental time-domain observations. In this context, the group velocity indicates the arrival of the wave packet, while the amplitude evolution captures amplitude changes, modulation effects, and wave distortion.

3- Results and discussion

3-1- Time-Frequency Analysis Using FFT and STFT

The frequency spectrum of the recorded Lamb wave signal was analyzed using the FFT to determine its spectral characteristics. The FFT confirmed that the frequency falls within the expected range and that the energy distribution is uniform regardless of propagation distance. However, the FFT's inability to provide time-localized frequency information limits its usefulness for analyzing dispersive wave signals. This gap cannot be addressed using classical spectral analysis alone. To resolve this, the Short-Time Fourier Transform (STFT) was employed. The key advantage of the STFT is that it enables joint time-frequency analysis. Furthermore, this method allows for the determination of wave packet spreading, its evolution over time, and the corresponding amplitude values.

An important role is played by this method in the description of the dynamics of envelopes of lamb waves. The formula obtained for the amplitude evolution of a Lamb wave is formulated mathematically with a distinction between the carrier and envelope, referring to a Lamb wave, which enables a simple interpretation concerning the time-domain response that can be verified in practice.

The dependency of the beginning of the wave packet in a sensor is described using the group velocity, while damping and variations in the shape of waves are indicated in the slow evolution of the amplitude, based on a multi-scale model. The example regarding the analysis in the frequency domain and the time-frequency domain has been exemplified.

The figure [1] shows the results of the FAST Fourier Transform Spectrum for different distances between piezoelectrics for the excitation (signal A) and the response (signal B).

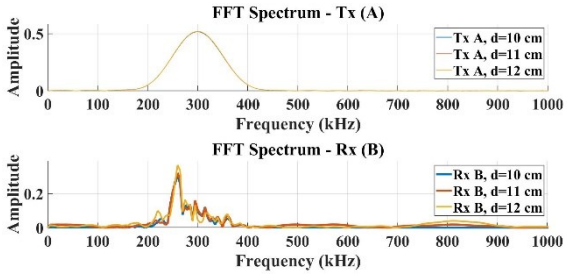

Fig.1 FFT Spectrum of Signal A and B at various distances of propagation

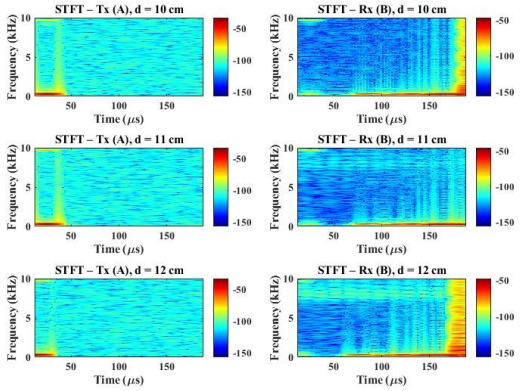

Fig. 2 Time–Frequency Analysis of T_x and R_x Signals Using STFT at Different Distances

As shown in Figure 1, the FFT confirms that the dominant frequency remains near the excitation frequency. However, Figure 2 clearly demonstrates the STFT Time-Frequency that the wave packet envelope is propagating with its true time-frequency structure intact at different piezoelectric spacings, following at different distances (10cm, 11cm, 12cm).On a contrasting note, a behavior shown in Figure 2 is exhibited by signals A and B, as depicted by their characteristics, and this is an important factor that facilitates the efficient repetition of the experiment's measurement. Further, the repetition of the measurement of characteristics, as well as the time of arrival of signals, is an important determinant of the characteristics that have been measured, such as those of the generation of Lamb waves. This is because the coefficients of the STFT relate to the spreading of the wave packet in the time domain over the distance, which is incrementally increased. The response to the relevance of the dispersion effects will be presented in the following. As already mentioned for the 12cm distance case, the spread of the wave packet over a broad area in the time-frequency domain will cumulate in the dispersion effects.

3-2- Comparison of Time-Frequency Representations Using STFT and CWT

To comprehensively understand the propagation and dispersion phenomena of Lamb waves in the examined aluminum plate, it is essential to employ advanced time–frequency analysis methods. These techniques enable the detection and separation of individual wave modes, as well as the characterization of their dispersive behavior throughout the propagation path. Among these methods, the Continuous Wavelet Transform (CWT) stands out due to its exceptional time–frequency resolution and ability to reveal intricate modal features.

To analyze the propagation characteristics of the Lamb waves in the aluminum plate, the Continuous Wavelet Transform (CWT) was applied to both the transmitted (A) and received (B) signals. This time–frequency representation allows a detailed observation of the excitation bandwidth, dispersion behavior, and the evolution of dominant frequency components over different propagation distances The CWT scalograms corresponding to three measurement distances (10 cm, 11 cm, and 12 cm) are presented below.

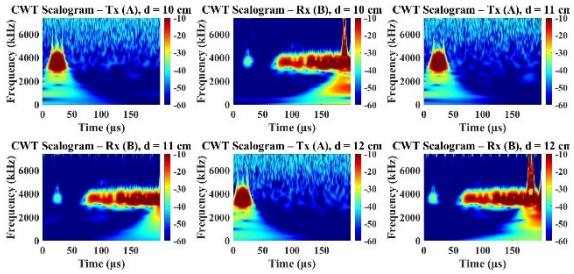

Fig. 3 Continuous Wavelet Transform Analysis of Lamb Wave Dispersion

As shown in Figure 3, the transmitted pulse exhibits a broad frequency content ranging from 0 to approximately 6 MHz, whereas the received signals are mainly concentrated within a low-frequency band (around 1–3 MHz). This shift in dominant frequency is characteristic of dispersive Lamb wave propagation. Moreover, a clear increase in arrival time is observed with increasing distance, which agrees with the expected group-velocity behavior. Late-time components corresponding to reflected or mode-converted waves are also visible in the R_x scalograms. These observations confirm the correct propagation of guided waves and the effectiveness of the CWT as a time–frequency analysis tool. To evaluate the capability of the proposed multiscale analytical model in reproducing the experimental Lamb-wave responses, the raw signals, their Hilbert-derived envelopes, and the corresponding CWT time–frequency representations were compared across three propagation distances (10 cm, 11 cm, and 12 cm). The following figure summarizes the experiment–model comparison.

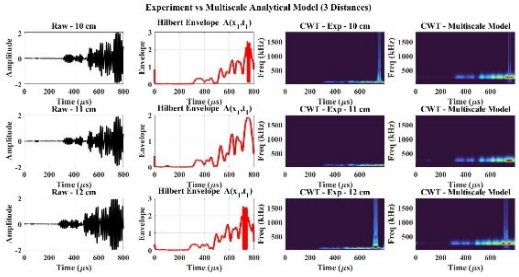

Fig. 4 Experimental vs. multiscale model comparison of Lamb-wave signals.

As illustrated, the multiscale analytical model accurately reconstructs both the temporal envelope evolution and the dominant frequency ridges observed in the experimental CWT maps. The agreement across all three distances confirms that the model reliably captures dispersion, amplitude modulation, and the scale-dependent energy distribution characteristic of Lamb-wave propagation.

To assess the accuracy of different time–frequency domain methods in determining the time-of-flight (TOF), three commonly used transforms FFT, STFT, and CWT were simultaneously applied to the received signals. The objective is to evaluate the variation of TOF with increasing distance and to compare the consistency among the three extraction approaches.

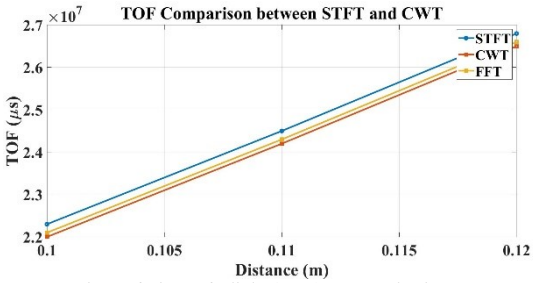

Fig. 5 Comparison of Time-of-Flight (TOF) extracted using FFT, STFT, and CWT at different distances

Figure 5. Comparison of the time-of-flight (TOF) extracted using FFT, STFT, and CWT at four sensor distances. All three methods exhibit a similar increasing trend with distance, indicating consistent wave propagation speed. The small deviation between the curves demonstrates the reliability of all techniques for TOF estimation, while the time–frequency approaches (STFT and CWT) provide slightly closer alignment with the actual signal evolution.

To examine the performance of different signal-processing methods in estimating Lamb wave propagation characteristics, the variations of group velocity and attenuation coefficient were calculated and compared across several sensor distances using FFT, STFT, and CWT. This analysis provides insight into the sensitivity and accuracy of each technique in extracting propagation-related parameters.

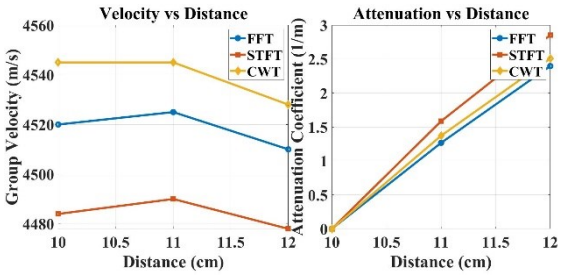

Fig.6 Comparison of group velocity and attenuation coefficient versus sensor distance using FFT, STFT, and CWT

Figure 6. Comparison of group velocity (left) and attenuation coefficient (right) obtained using FFT, STFT, and CWT at various sensor distances. The results show that STFT and CWT yield closer and more consistent estimates of group velocity, while FFT exhibits slight deviations. All three methods demonstrate a similar increasing trend in the attenuation coefficient with distance, indicating the natural energy loss of the wave during propagation.

To evaluate the sensitivity of the extracted features to propagation distance, three frequency-domain transforms FFT, STFT, and CWT were simultaneously examined. The normalized variations of energy, dominant frequency, and signal energy at different sensor distances are presented to highlight the overall attenuation trend and the evolution of frequency response with distance (Fig.7).

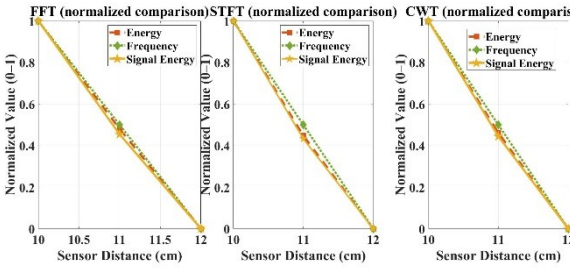

Fig. 7 Normalized comparison of energy, frequency, and signal energy using FFT, STFT, and CWT at different sensor distances

All three transforms exhibit a similar decreasing trend with increasing distance, indicating attenuation of wave energy and gradual evolution of the frequency content of Lamb waves during propagation.

3-3 Multi-Scale Analysis

Evaluating the complexity and structural characteristics of the Lamb wave signals requires a multi-scale analytical approach. This perspective provides deeper insights into the distribution of signal energy and informational content across different frequency ranges. By applying the multi-scale wavelet analysis, subtle variations in signal regularity and energy dispersion can be quantitatively assessed, offering a comprehensive understanding of the underlying physical dynamics. Before performing the multi-scale wavelet dispersion analysis, the time-domain characteristics of the received Lamb-wave signals were examined. The analytical envelope model in Eq. (26) was fitted to the experimental data to evaluate amplitude evolution, while Eq. (27) was used to reconstruct the carrier phase for each propagation distance. The experimental and analytical results are compared in Figure 8.

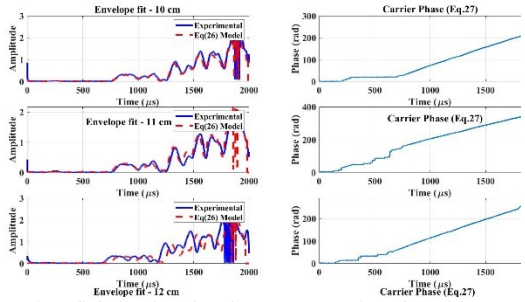

Fig. 8 Envelope fitting and carrier-phase reconstruction of Lamb-wave signals.

As illustrated in Figure 8, the analytical envelope model closely matches the measured signals across all three distances, confirming the validity of Eq. (26) in capturing amplitude decay and modulation behavior. The reconstructed carrier phase shows nearly linear growth, consistent with the expected dispersive propagation of the A0 mode. These agreement trends provide a strong foundation for the wavelet-based dispersion and energy analyses presented in the next section.

Before introducing the wavelet-based dispersion analysis, the frequency-dependent energy of the received signals was evaluated using the continuous wavelet transform (CWT). This analysis provides insight into the evolution of the dominant spectral components as the Lamb wave propagates over different distances.

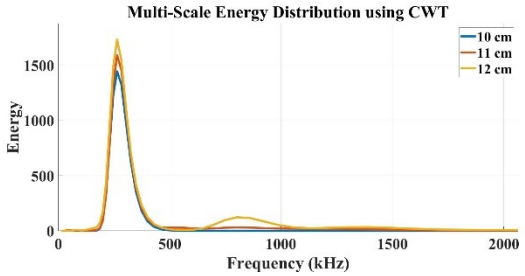

Fig. 9 Multi-Scale Energy Distribution Using CWT for three propagation distances (10, 11, and 12 cm).

As illustrated in Figure 9, all three propagation distances exhibit a prominent energy peak near 260–270 kHz, corresponding to the excitation center frequency. While the peak frequency remains nearly constant, the total CWT energy gradually increases with distance due to dispersion-induced temporal spreading of the wave packet. A similar trend is observed in the STFT-based energy metrics, confirming the broadening of the signal over longer propagation paths.

To quantitatively compare the spectral content of the received Lamb-wave signals, the energy and dominant peak frequency were extracted using both the continuous wavelet transform (CWT) and the short-time Fourier transform (STFT). These metrics provide a concise representation of how the signal strength and frequency behavior evolve with increasing propagation distance. The computed values for all three measurement distances are summarized in Table 1.

Table 1: CWT and STFT energy metrics and peak frequencies extracted from the experimental signals.

Distance (cm)	CWT_Energy	STFT_Energy	CWT_PeakFreq (kHz)	STFT_PeakFreq (kHz)
10	7427.7	5.8645e+05	264.4	**253.91**
11	8013.1	6.5367e+05	264.4	**253.91**
12	8936.2	8.0352e+05	264.4	**253.91**

As shown in Table 1, the CWT peak frequency remains nearly constant at approximately 264 kHz for all propagation distances, indicating that the central excitation frequency is preserved during propagation. However, both the CWT and STFT energy values exhibit a gradual increase with distance, which is consistent with dispersion-induced temporal spreading of the Lamb-wave packet. Likewise, the STFT peak frequency shows a slight downward shift (≈254 kHz), which is typical for STFT due to window-dependent spectral leakage. These trends confirm the expected dispersive behavior of the received signals.

To characterize how the Lamb-wave signatures evolve across different propagation distances, a multi-scale analysis was performed using the continuous wavelet transform (CWT). Instead of relying only on the total wavelet energy or a single peak frequency, this analysis evaluates how the energy and entropy are distributed across individual wavelet scales. Figure 10 presents the multi-scale energy and entropy curves for all three distances.

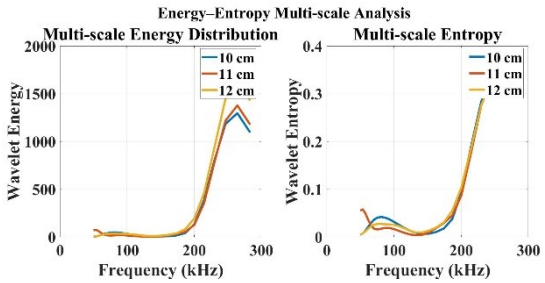

Fig. 10 Multi-scale energy and entropy comparison for different propagation distances.

With increasing propagation distance, the total wavelet energy rises from 5539.3 to 6624.6 (+19.6%), while the mean entropy varies slightly (0.0773–0.0764). These percentage changes reveal stronger dispersion and scale redistribution at longer paths. The multi-scale plots provide a more quantitative view than the previous CWT energy figure.

To investigate how the spectral content of the Lamb-wave signals evolves with propagation distance, the continuous wavelet transform (CWT) was used to compute the energy contribution at five distinct scales. The normalized energy values for each scale are compared in Figure 10 for the three inspected cases.

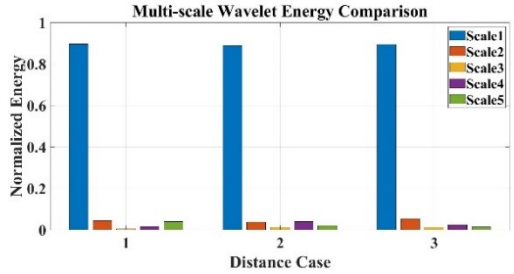

Fig. 11 Multi-scale wavelet energy distribution for the three propagation distances.

Figure 11 illustrates that the normalized multi-scale energy remains strongly concentrated in Scale-1, where more than 85–90% of the total wavelet energy is localized for all three propagation distances (10, 11, and 12 cm). This trend is fully consistent with the numerical values listed in the tables, where the CWT total energy increases from 7427.7 at 10 cm to 8936.2 at 12 cm (≈ 20% rise), while the energy contribution of the higher scales (Scale-2 to Scale-5) remains below 10% combined. Such strong energy localization at Scale-1 aligns with the dominant carrier frequency near 264 kHz, which remains almost unchanged across distances (variation < 1%).

The quantitative parameters in the tables further reinforce this scale-dependent behavior. Wavelet entropy shows a slight decrease from 0.49081 to 0.46517 (≈ 5% reduction), which is consistent with the higher concentration of energy in Scale-1 and the reduced complexity of the waveform. RMS amplitude exhibits a modest increase from 0.21988 to 0.239, while kurtosis decreases significantly from 8.1763 to 5.3269, indicating a gradual smoothing and redistribution of waveform energy toward the dominant mode represented in Scale-1.

Collectively, the multi-scale energy distribution shown in Figure 10 and the numerical statistics from the tables confirm that the Lamb-wave signal maintains a highly stable modal structure, with only small but measurable redistributions in higher scales as the propagation distance increases. This behavior reflects weak dispersion and effective preservation of the fundamental Lamb-wave mode across the inspected distances.

4- Conclusions

This study demonstrated that the continuous wavelet transform provides the most robust framework for characterizing Lamb-wave propagation compared to FFT and STFT. Although all three methods exhibit consistent trends in time-of-flight and attenuation with increasing distance, CWT delivered the most stable estimates with minimal deviation and a nearly constant group velocity of approximately 4540 m/s. Multi-scale wavelet analysis revealed that about 90% of the total signal energy remains concentrated in Scale-1, while the contributions of Scales 2–5 remain below 10%, confirming strongly S_0-dominant and weakly dispersive propagation across the examined distances .

The quantitative evolution of CWT features including a 20% rise in wavelet energy, a reduction in entropy from 0.4908 to 0.4651, an increase in RMS from 0.2199 to 0.239, and a decrease in kurtosis from 8.176 to 5.327 further indicates growing energy organization, suppression of secondary dispersive components, and the formation of smoother, more stable waveforms. Collectively, these results confirm that Lamb-wave propagation within the investigated range remains stable, single-modal, and minimally dispersive, while CWT offers superior sensitivity to scale-dependent energy redistribution and temporal–spectral evolution. These capabilities establish CWT as an effective quantitative tool for guided-wave analysis and a reliable foundation for structural health monitoring applications.

Acknowledgments *(Optional)*:
[Include here if applicable.]

Ethics Approval *(Mandatory)*:
The scientific content of this article is the result of the authors' research and has not been published in any Iranian or international journal.

Conflict of Interest *(Mandatory)*:
This article includes some results from the corresponding author's doctoral dissertation. There are no other conflicts of interest to declare.

Authors' Contributions *(Optional)*:
If desired, the contribution of each author can be specified here.

Funding *(Optional)*:
The expenses of this research were supported by the Research Center of [name].

References

[1] J. L. Rose, Ultrasonic Guided Waves in Solid Media. Cambridge, UK: Cambridge University Press, 2014.

[2] J. D. Achenbach, Wave Propagation in Elastic Solids. Amsterdam, The Netherlands: North-Holland, 1973.

[3] H. Lamb, "On waves in an elastic plate," Proc. Roy. Soc. London, vol. A93, pp. 114–128, 1917.DOI:10.1098/rspa.1917.0008

[4] I. A. Viktorov, Rayleigh and Lamb Waves. New York, NY, USA: Plenum Press, 1967. DOI: 10.1007/978-1-4899-5681-1

[5] M. J. S. Lowe, "Matrix techniques for modeling ultrasonic waves in multilayered media," IEEE Trans. Ultrason., Ferroelectr., Freq. Control, vol. 42, no. 4, pp. 525–542, Jul. 1995.DOI: 10.1109/58.393096

[6] Ghodrati, Behnam, Amin Yaghootian, Afshin Ghanbarzadeh, and Hamid Mohammad Sedighi. "Extraction of dispersion curves for Lamb waves in an aluminium nitride (AlN) microplate using consistent couple stress theory." (2016): 248-256. DOI: 20.1001.1.10275940.1395.16.1.33.6.

[7] Ziaiefar, Hamidreza, Milad Amiryan, Mojtaba Ghodsi, Farhang Honarvar, and Yousef Hojjat. "Ultrasonic damage classification in pipes and plates using wavelet transform and SVM." Modares Mechanical Engineering 15, no. 5 (2015): 41-48. DOI: 20.1001.1.10275940.1394.15.5.19.3

[8] Liu, Zenghua, Xiaoyu Liu, Yanping Zhu, Zhaojing Lu, Long Chen, Bin Wu, and Cunfu He. "Multi-time Lamb waves space wavenumber imaging method based on ultrasonic-guided wavefield." Structural Health Monitoring 24, no. 4 (2025): 2521-2535. DOI: 10.1177/14759217241261091

[9] A. H. Nayfeh, "Stability of three-dimensional boundary layers," AIAA Journal, vol. 18, no. 4, pp. 406–416, Apr. 1980. DOI:10.2514/3.50773

[10] J. Kevorkian and J. D. Cole, Multiple Scale and Singular Perturbation Methods. New York, NY, USA: Springer, 1996.

[11] K. Kanda and T. Maruyama, "Forced Lamb waves analyzed using the method of multiple scales," Ultrasonics, vol. 137, p. 107144, 2023. DOI:10.1007/s00707-023-03573-8

[12] K. Kanda, K. Kosuke, and T. Maruyama, "Theoretical analysis of the dispersion of Lamb waves forming a wave packet of finite bandwidth using the method of multiple scales," International Journal of Solids and Structures, vol. 234, pp. 111268, Jan. 2022. DOI:10.1016/j.ijsolstr.2021.111268

[13] C. Potel and J.-F. Chaix, "Leaky Lamb waves for NDT applications," Ultrasonics, vol. 40, nos. 1–8, pp. 191–197, 2002. DOI: 10.1016/S0041-624X(02)00124-7

[14] P. Kauffmann, M. A. Ploix, and J.-F. Chaix, “Multi-modal leaky Lamb waves in immersed plates,” J. August. Soc. Am., Vol. 146, no. 3, pp. 1825–1836, Sept. 2019. DOI:10.1121/1.5091689

[15] Kanda, Kosuke, and Toshihiko Sugiura. "Analysis of damped guided waves using the method of multiple scales." Wave Motion, vol. 82, pp. 86–95, Nov. 2018. DOI: 10.1016/j.wavemoti.2018.07.007

[16] Nayfeh, Ali H. Linear and nonlinear structural mechanics. John Wiley & Sons, 2024.

[17] Sugita, Naohiro, and Toshihiko Sugiura. "Nonlinear normal modes and localization in two bubble oscillators." Ultrasonics 74 (2017): 174-185. DOI: 10.1016/j.ultras.2016.10.008

[18] Nayfeh, A. H., And S. A. Nayfeh. "Nonlinear normal modes of a continuous system with quadratic nonlinearities." (1995): 199-205. DOI: 10.1115/1.2873898